



Accepted Article

Title: Activating effect of 3-benzylidene oxindoles on AMPK: from computer simulation to high-content screening

Authors: Daria S Novikova, Tatyana A Grigoreva, Gleb S Ivanov, Gerry Melino, Nickolai A Barlev, and Vyacheslav G Tribulovich

This manuscript has been accepted after peer review and appears as an Accepted Article online prior to editing, proofing, and formal publication of the final Version of Record (VoR). This work is currently citable by using the Digital Object Identifier (DOI) given below. The VoR will be published online in Early View as soon as possible and may be different to this Accepted Article as a result of editing. Readers should obtain the VoR from the journal website shown below when it is published to ensure accuracy of information. The authors are responsible for the content of this Accepted Article.

To be cited as: *ChemMedChem* 10.1002/cmdc.202000579

Link to VoR: <https://doi.org/10.1002/cmdc.202000579>

Activating effect of 3-benzylidene oxindoles on AMPK: from computer simulation to high-content screening

Daria S. Novikova,^{*[a]} Tatyana A. Grigoreva,^[a] Gleb S. Ivanov,^[a, c] Gerry Melino,^[b] Nickolai A. Barlev,^[c] and Vyacheslav G. Tribulovich^[a]

- [a] D. S. Novikova, 0000-0002-5310-4570, Dr. T. A. Grigoreva, 0000-0003-1271-0328, Dr. G. S. Ivanov, Dr. V. G. Tribulovich, 0000-0001-7723-4962
Laboratory of Molecular Pharmacology
Saint Petersburg State Institute of Technology (Technical University)
Moskovskii pr. 26, 190013 Saint Petersburg, Russia
E-mail: dc.novikova@gmail.com
- [b] Prof. Dr. G. Melino, 0000-0001-9428-5972
Department of Experimental Medicine and Surgery
University of Rome Tor Vergata
Via Montpellier 1, 00133 Rome, Italy
- [c] Dr. G. S. Ivanov, Prof. Dr. N. A. Barlev, 0000-0001-7111-2446
Laboratory of Regulation of Gene Expression
Institute of Cytology RAS
Tikhoretskii pr. 4, 194064 Saint Petersburg, Russia

Supporting information for this article is given via a link at the end of the document.

Abstract: AMP-activated protein kinase (AMPK) is currently the subject of intensive study and active discussions. AMPK performs its functions both at the cellular level, providing the switch between energy-consuming and energy-producing processes, and at the whole body level, particularly, regulating certain aspects of higher nervous activity and behavior. Control of such a 'main switch' compensates dysfunctions and associated diseases. In the present paper, we studied the binding of 3-benzylidene oxindoles to the kinase domain of the AMPK α -subunit, which is thought to prevent its interaction with the autoinhibitory domain and thus result in the AMPK activation. For this purpose, we developed the cellular test system based on the AMPKAR plasmid, which implements the FRET effect, synthesized a number of 3-benzylidene oxindole compounds and simulated their binding to various sites of the kinase domain. The most probable binding site for the studied compounds was established by the correlation of calculated and experimental data. The obtained results allow to analyze various classes of AMPK activators using virtual screening and HCS.

Introduction

Currently, AMP-activated protein kinase (AMPK) is considered as one of the key players in maintaining energy homeostasis. Numerous studies show that AMPK is the main regulator of energy balance at both the cellular and whole-body levels.^[1] Since the relevance of diseases associated with energy metabolism disturbances has been rapidly increased in recent decades, the regulation of the kinase activity of AMPK has become current therapeutic approach for the treatment and prevention of the considered group of diseases.^[2] AMPK functions as the energy regulator through the activation under energy stress. Being activated, AMPK blocks energy-consuming processes, such as protein synthesis, and activates processes aimed at energy production, which allows it to maintain the energy status of the organism at a certain level.^[3] It owes its name to AMP, its endogenous activator, whose concentration sharply increases under stress and energy depletion.^[4] Currently, the AMPK activation underlies the

therapeutic approach to the treatment of type 2 diabetes. So, metformin, whose beneficial effect is partially contributed by the activation of liver AMPK and suppression of gluconeogenesis, as well as increased glucose uptake in peripheral tissues, is the first-choice drug for type 2 diabetes patients.^[5]

AMPK is a heterotrimeric complex consisting of three subunits: α -subunit contains the main activation site, threonine residue (in the literature Thr172), and is responsible for the catalytic functions of the complex; regulatory β -subunit acts as a backbone of the complex, and also is involved in carbohydrate metabolism; regulatory γ -subunit is an energy sensor of the complex, having two competitive binding sites for adenine nucleotides (AMP/ADP/ATP).^[6]

Despite significant therapeutic interest in AMPK as a target^[7] and intensive study of its activation mechanisms in the last decade,^[6a, 8] a limited number of effective approaches have been developed to the design of compounds that activate the kinase.^[9] One can distinguish (1) targeting of AMP-binding sites, causing allosteric activation of AMPK;^[10] (2) development of compounds targeted at an alternative allosteric site (so-called ADaM site), identified by high-throughput screening;^[11] (3) blocking the function of the autoinhibitory domain (AID) of the kinase.^[12] The use of the latter approach is complicated by the lack of complete data on the structure of AMPK. X-ray structural data and NMR studies of individual domains allow us to fill in the gaps of the structural map of AMPK, as it was for the region of the autoinhibitory domain, whose structure has not been solved for a long time.^[13] However, in order to bring together experimental data on the structure of subunits within the complex, it is often necessary to use computer simulation, which allows to make certain conclusions about the functioning of the kinase complex as a whole with a certain degree of the reliability. Rational drug design is based on the consistent study of such relationships as disease–target, structure of target–ligand and, finally, structure–activity of the ligand. For the study of the last two relationships, the computer simulation of the ligand–receptor interaction and high-content screening (HCS) can be used as an effective set of tools. In this paper, we attempted to determine the binding site for the compounds activating AMPK by blocking

the autoinhibitory domain, and to establish a relationship between experimental data on the activity of these compounds towards AMPK and calculated results based on the interaction simulation of the studied compounds with the active site of the target. The specificity of 3-(benzylidene)indolin-2-one structure, which provides the possibility of binding to lipophilic areas of proteins, places increased demands on targeting of these compounds. The ability of a number of 3-(benzylidene)indolin-2-one derivatives to bind to the lipophilic cavity of the MDM2 protein, leading to activation of the p53 signaling pathway, was established.^[14] Correct application of the structure–activity relationship allows one to develop selective^[15] or multitarget small molecules based on indolin-2-one scaffold.^[16]

Results and Discussion

The autoinhibitory domain is one of the most interesting structural elements of AMPK used for drug development. The mobility of the autoinhibitory domain is functionally essential for the activation-inactivation process of the kinase complex. Being located within the catalytic α -subunit, the autoinhibitory domain directly affects the kinase function of AMPK. It was shown that the construct consisting of only the kinase and autoinhibitory domains is inactive, while the deletion of a small region of the autoinhibitory domain converts the catalytic α -subunit into the permanently active state.^[17] The search for small molecule compounds that block intramolecular protein-protein interaction between the autoinhibitory and kinase domains seems to be a promising approach in the development of active and selective compounds for the AMPK activation.

The choice of an experimental model that quantitatively fixes the effect of a small molecule compound on the target is a required step in the rational drug design in addition to the druggable target suitable for the design of drugs. For this study, we chose the FRET (Förster resonance energy transfer) method. Determination of the kinase activity using FRET biosensors introduced into living cells is a fairly common method in molecular biology.^[18] It is based on the phenomenon of energy transfer between two chromophores, in which fluorescence of the donor chromophore is quenched, while the acceptor chromophore emits fluorescence in the long-wave region. The closure of the chromophores is required for the transfer, which is achieved by the presence of special protein sensors sensitive to the studied process (Fig. 1). The most common chromophore pair is cyan (CFP) and yellow (YFP) fluorescent protein.

The first FRET biosensor, designed specifically for the study the AMPK activation process, was AMPKAR (AMPK activity reporter).^[19] This construct consists of a modified version of cyan fluorescent protein (eCFP) as the donor fluorophore, the FHA1 domain^[20] that recognizes threonine residue phosphorylation (ligand domain), the protein substrate of AMPK (sensory domain) and a modified version of yellow fluorescent protein (Venus) as the acceptor fluorophore. The protein sequence GSGEGSTKMRRVAT*LVDLGTGGSEL (where T* is threonine, phosphorylated by AMPK), detected in the screening of the peptide library and showed specificity for AMPK, was used as the AMPK substrate. The construct obtained by the authors was used to study the process of the AMPK activation in a single cell (Single Cell Analysis) using modern microfluidic technique.

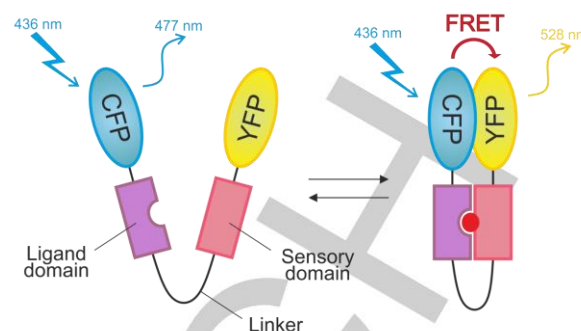


Figure 1. FRET biosensor based on cyan (CFP) and yellow (YFP) fluorescent protein.

The degree of the AMPK activation is usually assessed either by the phosphorylation degree of the main substrates of the kinase^[21] or by physiological effects such as decreased lipogenesis,^[10] increased glucose uptake,^[22] decreased glucose production^[23] and others. In the case of AMPKAR, one can most accurately assess the AMPK activity without the need to consider additional pathways of phosphorylation and dephosphorylation of AMPK substrates or complicated mechanisms of integral effects.^[24]

We tried to adapt the described system for HCS assays using the Operetta High-Content Imaging System, which allows conducting a wide range of such studies.^[25] The FRET biosensor was used to obtain a cellular test system for evaluating the ability of small molecule compounds to activate AMPK. H1299 (human non-small cell lung cancer) cell line was laid in the basis of the test system. Non-small cell carcinoma is the most common type among lung cancers and represented by LKB1 positive cells, which are used in AMPK-related studies.^[26] H1299 cells, which stably express the AMPKAR construct, were obtained by lentiviral infection. The most stable clones with the maximum fluorescence signal were recruited as the test system for AMPK activation. To validate the sensitivity of modified cell line under HCS conditions known activators were used: AMP, endogenous AMPK activator, and 5-aminoimidazole-4-carboxamide riboside (AICAR), a synthetic AMPK activator, which reproduces the effects of extracellular AMP.^[27] According to the published data, AMP causes up to 10-fold activation of the AMPK complex depending on the subunit composition. It is believed that activation of intracellular AMPK through increasing the concentration of extracellular AMP is achieved due to dephosphorylation by 5'-nucleotidase (CD73), the use of adenosine transport and subsequent intracellular monophosphorylation.^[28] AICAR is thought to be an incomplete AMP mimetic, and it is incapable of showing the same activating effect *in vivo* as AMP.^[29] The treatment with these activators at the concentration of 1 mM allowed to observe the activating effect (Fig. 2). The small value of the change in the YFP to CFP signal ratio (Δ FRET) is due to the specificity of the FRET effect, which is the energy transfer through the space and is inversely related to the sixth degree of the distance between the sensors. In addition, it should be noted that the activating effect strongly depends on the initial (basal) level of the AMPK activity.

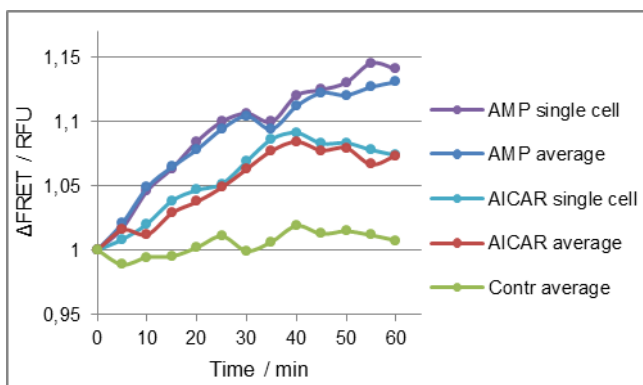


Figure 2. Response of AMPK activation cell model under the treatment with AMP and AICAR at the concentration of 1 mM. Curves 'AMP single cell' and 'AICAR single cell' correspond to the FRET effect measured for an individual cell. Curves 'AMP average' and 'AICAR average' correspond to the average FRET effect of 8 fields within the well.

We measured the FRET effect for both individual cells, which were monitored throughout the experiment, and in the HCS mode by the average signal of 8 fields within the well of a 96-well plate. As can be seen from Fig. 2, both modes of the study demonstrate a high degree of similarity, which indicates a correct transfer of the single cell technique to HCS.

The prospects of the approach to the AMPK activation by blocking the function of the autoinhibitory domain have been considered for a long time. The first advance in this area is compound PT1, which was identified by screening the library of 3600 compounds and showed the ability to activate the single catalytic α -subunit beyond the heterotrimeric AMPK complex.^[30] Due to an extremely low bioavailability of PT1, efforts were made to develop similar small molecule compounds. Thus 3-benzylidene oxindoles were designed, which are the most interesting among the developed activators of this type showing significant activity towards AMPK.^[31] However, the AMPK binding site has not been established for this class of compounds yet.

In order to develop a computational model for the search and optimization of AMPK activators, which can act as autoinhibitory domain blockers, we tried to determine the binding site for 3-benzylidene oxindole compounds. As starting point we used the most active 3-benzylidene oxindole compound, which is often referred in the literature as C24 (or YLF-466D). The ability to highly activate AMPK in both *in vitro* and *in vivo* experiments has been demonstrated for this compound.^[31, 32] We performed molecular docking of C24 to the catalytic α -subunit of AMPK. The docking area, further referred to as the α A site, was chosen based on available X-ray diffraction data and data concerning the effects of proteolytic mutations on the autoinhibitory domain interactions,^[8, 17b, 33] and also using the results of our simplified

Table 1. Calculated lipophilicity (logP), scoring function (GoldScore) of binding to different sites and experimental activating effect (Δ FRET) measured in the cell model for series of 3-benzylidene oxindole compounds.

Compound	logP		GoldScore			Δ FRET
	ChemOffice	AlogPS 2.1	α A site	α B site	α AB site	
3a	2.36	2.80	40.53	41.92	41.36	1.04±0.02
3b	2.78	3.33	42.50	39.98	43.82	1.01±0.02
3c	2.92	3.58	38.83	39.27	43.97	1.17±0.02
3d	2.92	3.60	38.91	39.49	41.55	1.08±0.02
3e	3.19	3.54	38.80	39.48	44.36	1.12±0.02
3f	2.92	3.50	41.54	40.73	44.45	1.16±0.03
3g	3.48	4.10	40.39	41.4	43.75	1.21±0.02
3h	3.57	3.93	34.93	42.26	44.41	1.26±0.03
3i	4.12	4.54	37.63	44.59	45.62	1.35±0.03
3j	4.12	4.54	37.19	41.81	46.33	1.47±0.02
3k	4.39	3.90	43.53	45.54	50.45	1.53±0.03
3l	4.94	4.50	45.21	45.82	50.81	1.55±0.03
3m	4.94	4.46	46.03	46.09	51.63	1.71±0.03
3n	5.59	4.87	46.25	47.74	54.51	1.89±0.04
3o (C24)	6.15	5.62	47.44	49.27	56.98	2.00±0.04
3p	6.15	5.62	48.33	48.62	54.66	1.83±0.04

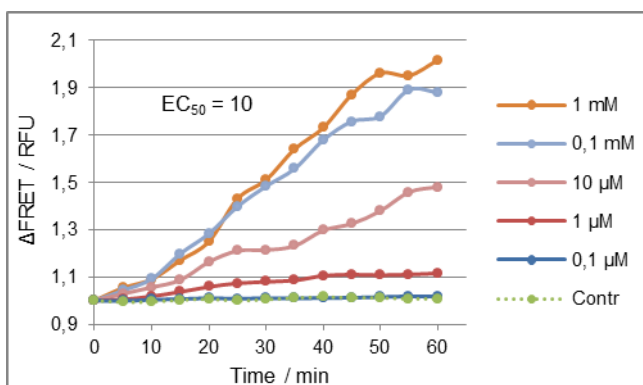


Figure 4. Curves of AMPK activation under the treatment with C24 at different concentrations used to determine the value of EC_{50} for the developed cell model.

and Val82. The carboxyl group forms a hydrogen bond with Lys69.

To develop a working model reflecting the relationship between experimental and calculated data for autoinhibitory domain blockers, we designed a series of 3-benzylidene oxindole compounds with different activating potential and studied their activity using the cellular test system.

The simplest active compound of 3-benzylidene oxindoles is compound **3a**. Its synthesis is carried out by condensation of 2-oxindole with acetophenone, subsequent alkylation of the nitrogen atom with methyl bromoacetate and alkaline hydrolysis (Scheme 1).^[36] Despite considerable structural similarity with compound **3a**, synthesis of compound C24 is carried out according to a more complicated scheme^[31] due to low conversion upon condensation of 4-chlorobenzophenone with 2-oxindole. However, we developed a method of condensation, which allows to obtain benzophenone derivatives according to the same scheme.^[37] Therefore, we synthesized several new compounds between **3a** and C24 with intermediate activity according to Scheme 1. The lipophilicity of molecule binding fragments was the main varying parameter when changing the structure from **3a** to C24 (Table 1). The target activity of the

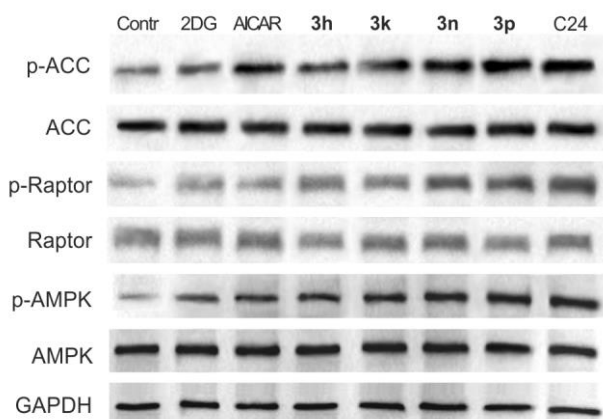


Figure 5. Western blot analysis of 3-benzylidene oxindole compounds (incubation for 1 h at the concentration of 0.1 mM). 2-Deoxyglucose (2DG) and AICAR were used as reference AMPK activators at the concentration of 20 mM and 2.5 mM, respectively.

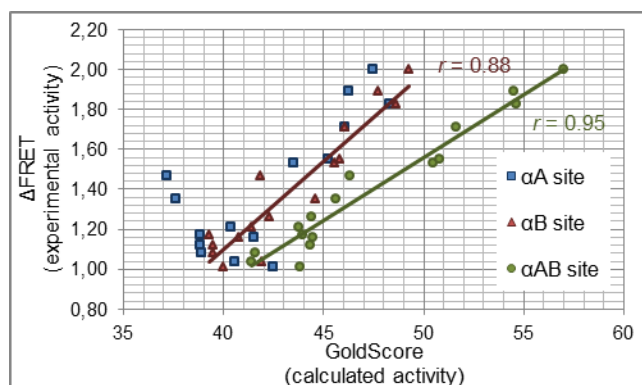


Figure 6. Correlation of experimental and calculated data on the interaction of 3-benzylidene oxindoles with different sites of AMPK α -subunit.

obtained series of 3-benzylidene oxindoles was evaluated in the cellular test system; the average values of the change in the FRET effect under the treatment of the studied compounds are given in Table 1. A more detailed study of the activating effect of C24 yielded the EC_{50} value (Fig. 4).

To confirm that the observed FRET effect is mediated by AMPK, *in vitro* experiments by Western blot were carried out. In this case, the ability of the compounds to both stimulate AMPK phosphorylation at the activation site and to phosphorylate the main downstream targets was evaluated. The results obtained (Fig. 5) were in good agreement with those obtained in the cellular test system.

All the compounds and considered interaction sites were used in the docking study (Table 1). Even though the minimum activity was predicted for propiophenone derivative using the αA site, the GoldScore values for more lipophilic derivatives were not consistent with the data of the biological experiment. Docking to the αB site showed significantly better agreement with the experimental data (Fig. 6). Obviously, the absence of a correlation between calculated and experimental data for the αA site may lead to the loss of highly active compounds during virtual screening of large libraries of compounds, as well as to the choice of incorrect directions for the optimization of the structure of small molecule compounds.

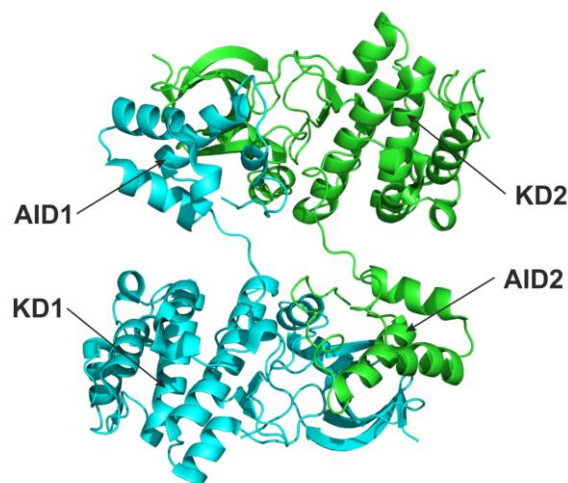


Figure 7. Cartoon representation of KD-AID dimer (PDB id 4RED).

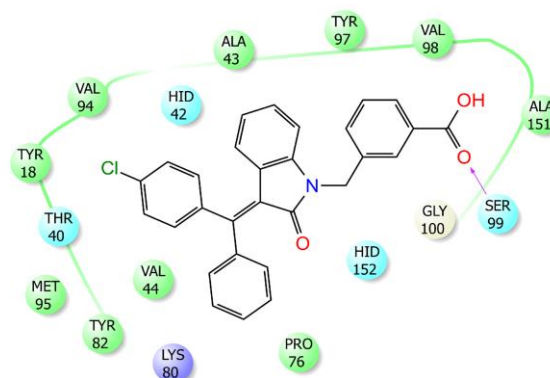
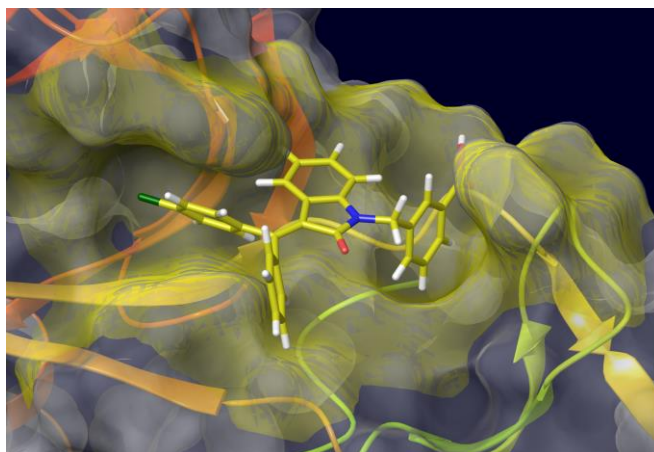


Figure 8. Proposed α AB site of C24 interaction with catalytic subunit of AMPK (PDB id 4RED) and ligand interaction diagram.

The search for resolved structures of the kinase domain (KD) of AMPK led us to the 4RED structure, which represents not full-length AMPK complex, but the KD-AID dimer.^[33] This dimer of the α -subunit is folded so that the autoinhibitory domain of one subunit interacts with the kinase domain of another (Fig. 7). The tendency to dimerization observed in 4RED, probably, determines the lack of the activity of a single α -subunit, which is in an inactive state due to the fixed conformation.

Changes in the kinase domain structure of the 4RED monomer, associated with an untwisting of the α -helix in the Ile65–Leu70 region, result in a change in the tertiary structure of the hydrophobic binding cavity compared to 4QFG. The hybrid binding site α AB, which combines the properties of both α A and α B sites, considered previously, is formed (Fig. 8).

Using the 4RED structure and the proposed binding site for our virtual experiments, we obtained good correlation between the calculated and experimental data (Fig. 6). The computer simulation of C24 binding showed the presence of a large number of lipophilic contacts for phenyl fragments of the compound: Tyr18, Ala43, Val44, Pro76, Val94, Tyr97, Val98, and hydrogen bonding of the carboxyl group with Ser99 (Fig. 8). The observed mode of C24 binding quite fully realizes both its lipophilic potential and the binding ability of the carboxyl group.

Conclusions

In summary, the cell model based on the AMPKAR plasmid was developed and validated for HCS. The experiments were carried out in living cells, the FRET effect arising from the treatment with small molecule compounds was measured in real time. The ability of 3-benzylidene oxindoles to bind to the kinase domain of the AMPK α -subunit for preventing its interaction with the autoinhibitory domain was simulated. Structures of the kinase domain obtained from the Protein Data Bank (PDB id 4QFG and 4RED) were used as receptors for the considered ligand–receptor system. The preferred binding site of the α -subunit for the studied small molecule ligands was determined by the correlation of quantitative parameters of computer simulation and experimental data on the AMPK activation. The lipophilic

nature of the interaction of 3-benzylidene oxindoles with the kinase domain of AMPK was established.

The obtained data allow both to optimize the studied series of 3-benzylidene oxindoles and to analyze diverse libraries of compounds using virtual screening and HCS.

Experimental Section

Computer simulation

Molecular docking of the studied compounds was performed on a HP Z8 G4 (nVidia Quadro RTX 5000) workstation using the CCDC GOLD Suite v5.2.2 software package.^[38] The X-ray crystallographic structures of the AMPK kinase domain were obtained from the Protein Data Bank (PDB id 4QFG^[8] and 4RED^[33]). The structure of the kinase domain was prepared for docking studies by adding hydrogen atoms with the standard geometry. The binding affinity of the studied compounds was evaluated by the GoldScore fitness function. The binding poses that correspond to the highest values of GoldScore were visualized to confirm the accuracy of the binding. The GoldScore values obtained for different active sites were used to construct correlations between experimental and calculated data.

The lipophilicity (lopP) of the studied compounds was calculated using ChemOffice software package and AlogPS 2.1 online service.^[39]

Chemistry

2-Oxindoles obtained according to the known procedure^[40] were used as starting compounds. Other starting compounds and reagents used were commercially available. Synthesis of the studied compounds was carried out in accordance with Scheme 1.

The reactions were monitored by TLC on Silica gel 60 F254 plates (Merk) in hexane-ethyl acetate. Purification of the products was carried out using an Isolera Four flash chromatograph on SNAP KP-Sil 100g cartridges (Biotage) using hexane-ethyl acetate eluent.

¹H and ¹³C NMR spectra were recorded on a Bruker Avance III 400 (400 MHz) device in DMSO-*d*₆. Mass spectra were recorded on a LCMS-2020 (Shimadzu) with a single quadrupole detector under positive mode; electrospray ionization (ESI).

General procedure for synthesis of 3-benzylidene oxindoles 1a-g. 2-Oxindole or substituted oxindole (0.075 mol) was suspended in 200 mL of toluene. The corresponding ketone (0.09 mol, 1.2 equiv.), 16.5 mL of pyrrolidine (0.15 mol, 2 equiv.) were added to the suspension. The reaction mixture was refluxed with the Dean-Stark trap for 0.5–4 hours. The reaction was monitored by TLC. Then the mixture was cooled, the solvent was evaporated under reduced pressure. The residue was treated with a small amount of ethyl acetate and then filtered off, or recrystallized from n-hexane/ethyl acetate, or purified by flash chromatography using n-hexane/ethyl acetate eluent.

Analytical data for compounds **1a-g** are given in Supporting Information.

General procedure for synthesis of 3-benzylidene oxindoles 1h-j. 2-Oxindole (4 g, 0.03 mol) was dissolved in dried and freshly distilled THF, the corresponding benzophenone (0.036 mol, 1.2 equiv.), pyridine (4.8 mL, 0.06 mol, 2 equiv.) and aluminum isopropoxide (18.4 g, 0.09 mol, 3 equiv.) were added. The reaction mixture was heated to 40°C and kept overnight. Then the reaction mixture was quenched with 3% Na₂CO₃ solution, extracted with ethyl acetate, dried over anhydrous Na₂SO₄ and evaporated under reduced pressure. The product (or mixture of products) was isolated by flash chromatography with n-hexane/ethyl acetate eluent.

Analytical data for compounds **1h-j** are given in Supporting Information.

General procedure for synthesis of N-substituted 3-benzylidene oxindoles 2a-p. Compound **1a-j** (0.01 mol) was dissolved in 50 mL THF and cooled on ice, 0.5 g sodium hydride (60%, 0.0125 mol, 1.25 equiv.) was added under stirring. The mixture was kept for 30 min at rt. Then methyl bromoacetate or methyl 3-(bromomethyl)benzoate (0.014 mol, 1.4 equiv.) dissolved in 10 mL THF was added dropwise. The reaction mixture was stirred for 3 h, the solvent was then evaporated under reduced pressure, 50 mL water was added to the residue. The resulting precipitate was filtered off, dried, and the product was isolated by flash chromatography.

Analytical data for compounds **2a-p** are given Supporting Information.

General procedure for synthesis of acids 3a-p. Compound **2a-p** (0.01 mol) in 50 mL THF was added to lithium hydroxide (2.4 g, 0.1 mol) dissolved in 50 mL water. The reaction mixture was stirred for 10–30 min (for **2h-j** and **2n-p** –12 h) at rt, the organic solvent was then distilled off. The mixture was acidified with 15% HCl, the precipitate was filtered off, washed with 50 mL water and dried. The crude product was purified by recrystallization from ethyl acetate.

(E)-2-(2-oxo-3-(1-phenylethylidene)indolin-1-yl)acetic acid (3a): yellow crystalline solid in 94% yield; mp 213–215°C; ¹H NMR (400 MHz, DMSO-*d*₆) δ (ppm): 7.57–7.47 (m, 3H), 7.35 (d, *J* = 6.7 Hz, 2H), 7.12 (t, *J* = 7.6 Hz, 1H), 6.91 (d, *J* = 7.8 Hz, 1H), 6.62 (t, *J* = 7.6 Hz, 1H), 6.04 (d, *J* = 7.7 Hz, 1H), 4.50 (s, 2H), 2.75 (s, 3H); ¹³C NMR (100 MHz, DMSO-*d*₆) δ (ppm): 169.97, 167.55, 155.40, 142.83, 141.64, 129.75, 129.02, 128.77, 126.67, 122.78, 122.47, 122.23, 121.65, 108.92, 41.19, 22.90; MS (ESI) *m/z* 294.1 [M + H]⁺.

(E)-2-(2-oxo-3-(1-phenylpropylidene)indolin-1-yl)acetic acid (3b): yellow crystalline solid in 95% yield; mp 197–198°C; ¹H NMR (400 MHz, DMSO-*d*₆) δ (ppm): 7.55–7.45 (m, 3H), 7.28 (d, *J* = 6.7 Hz, 2H), 7.08 (t, *J* = 7.7 Hz, 1H), 6.80 (d, *J* = 7.8 Hz, 1H), 6.56 (t, *J* = 7.7 Hz, 1H), 5.95 (d, *J* = 7.7 Hz, 1H), 4.45 (s, 2H), 3.28 (q, *J* = 7.4 Hz, 2H), 1.07 (t, *J* = 7.4 Hz, 3H); ¹³C NMR (100 MHz, DMSO-*d*₆) δ (ppm): 169.97, 167.17, 160.79, 141.80, 141.07, 129.68, 128.96, 128.81, 127.11, 122.56, 122.44, 122.28, 121.65, 108.92, 41.20, 27.76, 12.21; MS (ESI) *m/z* 308.2 [M + H]⁺.

(E)-2-(5-chloro-2-oxo-3-(1-phenylethylidene)indolin-1-yl)acetic acid (3c): yellow crystalline solid in 92% yield; mp 243–245°C; ¹H NMR (400 MHz, DMSO-*d*₆) δ (ppm): 7.61–7.52 (m, 3H), 7.36 (dd, *J* = 7.8 Hz, 1.5 Hz,

2H), 7.20 (dd, *J* = 8.4, 2.0 Hz, 1H), 7.01 (d, *J* = 8.4 Hz, 1H), 5.87 (d, *J* = 1.9 Hz, 1H), 4.54 (s, 2H), 2.76 (s, 3H); ¹³C NMR (100 MHz, DMSO-*d*₆) δ (ppm): 169.82, 167.19, 157.83, 142.29, 140.41, 129.88, 129.33, 128.23, 126.50, 125.73, 123.81, 122.29, 122.07, 110.46, 41.32, 23.00; MS (ESI) *m/z* 328.1 [M + H]⁺.

(E)-2-(6-chloro-2-oxo-3-(1-phenylethylidene)indolin-1-yl)acetic acid (3d): yellow crystalline solid in 91% yield; mp 213–214°C; ¹H NMR (400 MHz, DMSO-*d*₆) δ (ppm): 7.58–7.48 (m, 3H), 7.36 (d, *J* = 7.1 Hz, 2H), 7.16 (s, 1H), 6.72 (d, *J* = 8.3 Hz, 1H), 5.98 (d, *J* = 8.3 Hz, 1H), 4.55 (s, 2H), 2.73 (s, 3H); ¹³C NMR (100 MHz, DMSO-*d*₆) δ (ppm): 169.81, 167.52, 156.58, 142.99, 142.48, 133.22, 129.81, 129.25, 126.64, 123.50, 121.91, 121.35, 121.07, 109.45, 41.43, 22.99; MS (ESI) *m/z* 328.1 [M + H]⁺.

(E)-2-(5-bromo-2-oxo-3-(1-phenylethylidene)indolin-1-yl)acetic acid (3e): yellow crystalline solid in 89% yield; mp 245–247°C; ¹H NMR (400 MHz, DMSO-*d*₆) δ (ppm): 7.61–7.52 (m, 3H), 7.36 (dd, *J* = 7.7, 1.5 Hz, 2H), 7.32 (dd, *J* = 8.4, 2.0 Hz, 1H), 6.96 (d, *J* = 8.4 Hz, 1H), 6.01 (d, *J* = 1.9 Hz, 1H), 4.53 (s, 2H), 2.76 (s, 3H); ¹³C NMR (100 MHz, DMSO-*d*₆) δ (ppm): 169.76, 167.07, 157.82, 142.29, 140.77, 131.01, 129.85, 129.31, 126.50, 125.12, 124.26, 121.98, 113.53, 110.95, 41.29, 22.98; MS (ESI) *m/z* 372.0 [M + H]⁺.

(E)-2-(3-(1-(4-chlorophenyl)ethylidene)-2-oxoindolin-1-yl)acetic acid (3f): yellow crystalline solid in 93% yield; mp 230–232°C; ¹H NMR (400 MHz, DMSO-*d*₆) δ (ppm): 7.57 (d, *J* = 8.4 Hz, 2H), 7.39 (d, *J* = 8.4 Hz, 2H), 7.14 (t, *J* = 7.5 Hz, 1H), 6.90 (d, *J* = 7.8 Hz, 1H), 6.68 (t, *J* = 7.5 Hz, 1H), 6.15 (d, *J* = 7.7 Hz, 1H), 4.49 (s, 2H), 2.73 (s, 3H); ¹³C NMR (100 MHz, DMSO-*d*₆) δ (ppm): 169.94, 167.43, 153.76, 141.75, 141.50, 133.75, 129.84, 128.93, 123.12, 122.45, 122.00, 121.80, 109.02, 41.21, 22.70; MS (ESI) *m/z* 328.1 [M + H]⁺.

(E)-2-(5-chloro-3-(1-(4-chlorophenyl)ethylidene)-2-oxoindolin-1-yl)acetic acid (3g): yellow crystalline solid in 90% yield; mp 226–228°C; ¹H NMR (400 MHz, DMSO-*d*₆) δ (ppm): 7.66 (d, *J* = 8.4 Hz, 2H), 7.44 (d, *J* = 8.3 Hz, 2H), 7.23 (dd, *J* = 8.4, 2.0 Hz, 1H), 7.03 (d, *J* = 8.4 Hz, 1H), 5.97 (d, *J* = 1.9 Hz, 1H), 4.54 (s, 2H), 2.74 (s, 3H); ¹³C NMR (100 MHz, DMSO-*d*₆) δ (ppm): 169.78, 167.08, 156.30, 140.96, 140.53, 134.06, 129.96, 128.84, 128.47, 125.77, 123.57, 122.33, 122.16, 110.64, 41.34, 22.85; MS (ESI) *m/z* 362.1 [M + H]⁺.

2-(3-(diphenylmethylene)-2-oxoindolin-1-yl)acetic acid (3h): yellow crystalline solid in 95% yield; mp 244–246°C; ¹H NMR (400 MHz, DMSO-*d*₆) δ (ppm): 7.53–7.48 (m, 3H), 7.34–7.25 (m, 7H), 7.08 (t, *J* = 7.6 Hz, 1H), 6.74 (d, *J* = 7.8 Hz, 1H), 6.60 (t, *J* = 7.6 Hz, 1H), 6.09 (d, *J* = 7.7 Hz, 1H), 4.07 (s, 2H); ¹³C NMR (100 MHz, DMSO-*d*₆) δ (ppm): 165.72, 153.01, 144.00, 141.80, 140.38, 129.95, 129.68, 129.38, 129.28, 128.84, 128.73, 128.07, 124.74, 122.66, 122.60, 121.01, 109.41, 43.54; MS (ESI) *m/z* 356.2 [M + H]⁺.

(E)-2-(3-((4-chlorophenyl)(phenyl)methylene)-2-oxoindolin-1-yl)acetic acid (3i): yellow crystalline solid in 94% yield; mp 216–218°C; ¹H NMR (400 MHz, DMSO-*d*₆) δ (ppm): 7.59 (d, *J* = 8.3 Hz, 2H), 7.38–7.33 (m, 5H), 7.30–7.25 (m, 2H), 7.20 (t, *J* = 7.7 Hz, 1H), 6.97 (d, *J* = 7.9 Hz, 1H), 6.75 (t, *J* = 7.7 Hz, 1H), 6.29 (d, *J* = 7.7 Hz, 1H), 4.44 (s, 2H); ¹³C NMR (100 MHz, DMSO-*d*₆) δ (ppm): 169.86, 165.89, 152.67, 142.90, 140.22, 139.87, 134.42, 130.98, 130.08, 129.85, 129.72, 129.26, 128.23, 124.23, 122.86, 122.50, 121.91, 109.27, 41.30; MS (ESI) *m/z* 390.1 [M + H]⁺.

(Z)-2-(3-((4-chlorophenyl)(phenyl)methylene)-2-oxoindolin-1-yl)acetic acid (3j): yellow crystalline solid in 95% yield; mp 195–196°C; ¹H NMR (400 MHz, DMSO-*d*₆) δ (ppm): 7.55–7.50 (m, 3H), 7.42 (d, *J* = 8.5 Hz, 2H), 7.36–7.32 (m, 2H), 7.31 (d, *J* = 8.5 Hz, 2H), 7.19 (t, *J* = 7.6 Hz, 1H), 6.96 (d, *J* = 7.8 Hz, 1H), 6.69 (t, *J* = 7.6 Hz, 1H), 6.19 (d, *J* = 7.7 Hz, 1H), 4.44 (s, 2H); ¹³C NMR (100 MHz, DMSO-*d*₆) δ (ppm): 169.85, 166.00, 152.55, 142.90, 141.01, 138.93, 133.91, 131.86, 129.81, 129.73,

128.83, 128.27, 124.38, 122.96, 122.55, 121.82, 109.25, 41.31; MS (ESI) m/z 390.1 [M + H]⁺.

(E)-3-((2-oxo-3-(1-phenylethylidene)indolin-1-yl)methyl)benzoic acid (3k): yellow crystalline solid in 93% yield; mp 193–194°C; ¹H NMR (400 MHz, DMSO-*d*₆) δ (ppm): 7.93 (s, 1H), 7.86 (d, *J* = 7.6 Hz, 1H), 7.60 (d, *J* = 7.5 Hz, 1H), 7.57–7.45 (m, 4H), 7.38 (d, *J* = 7.1 Hz, 2H), 7.09 (t, *J* = 7.6 Hz, 1H), 6.91 (d, *J* = 7.8 Hz, 1H), 6.62 (t, *J* = 7.6 Hz, 1H), 6.03 (d, *J* = 7.7 Hz, 1H), 5.06 (s, 2H), 2.79 (s, 3H); ¹³C NMR (100 MHz, DMSO-*d*₆) δ (ppm): 167.61, 167.56, 155.81, 142.85, 141.30, 137.86, 132.29, 131.64, 129.72, 129.45, 129.03, 128.81, 128.49, 126.74, 122.80, 122.63, 122.44, 121.77, 109.14, 42.55, 23.01; MS (ESI) m/z 370.2 [M + H]⁺.

(E)-3-((5-chloro-2-oxo-3-(1-phenylethylidene)indolin-1-yl)methyl)benzoic acid (3l): yellow crystalline solid in 92% yield; mp 217–219°C; ¹H NMR (400 MHz, DMSO-*d*₆) δ (ppm): 7.91 (s, 1H), 7.86 (d, *J* = 7.7 Hz, 1H), 7.60–7.54 (m, 4H), 7.49 (t, *J* = 7.6 Hz, 1H), 7.40 (dd, *J* = 7.7, 1.4 Hz, 2H), 7.17 (dd, *J* = 8.4, 2.0 Hz, 1H), 6.94 (d, *J* = 8.4 Hz, 1H), 5.88 (d, *J* = 2.0 Hz, 1H), 5.06 (s, 2H), 2.81 (s, 3H); ¹³C NMR (100 MHz, DMSO-*d*₆) δ (ppm): 167.54, 167.26, 158.21, 142.32, 140.02, 137.52, 132.25, 131.65, 129.85, 129.50, 129.35, 128.89, 128.48, 128.28, 126.57, 125.88, 124.07, 122.46, 122.10, 110.56, 42.62, 23.11; MS (ESI) m/z 404.2 [M + H]⁺.

(E)-3-((3-(1-(4-chlorophenyl)ethylidene)-2-oxoindolin-1-yl)methyl)benzoic acid (3m): yellow crystalline solid in 95% yield; mp 240–242°C; ¹H NMR (400 MHz, DMSO-*d*₆) δ (ppm): 7.91 (s, 1H), 7.85 (d, *J* = 7.7 Hz, 1H), 7.63–7.58 (m, 3H), 7.48 (t, *J* = 7.9 Hz, 1H), 7.44 (d, *J* = 8.3 Hz, 2H), 7.12 (t, *J* = 7.7 Hz, 1H), 6.93 (d, *J* = 7.8 Hz, 1H), 6.70 (t, *J* = 7.7 Hz, 1H), 6.12 (d, *J* = 7.7 Hz, 1H), 5.06 (s, 2H), 2.77 (s, 3H); ¹³C NMR (100 MHz, DMSO-*d*₆) δ (ppm): 167.58, 167.49, 154.23, 141.54, 141.38, 137.77, 133.74, 132.23, 131.78, 129.84, 129.43, 129.03, 128.82, 128.47, 123.11, 122.59, 122.19, 121.95, 109.28, 42.56, 22.83; MS (ESI) m/z 404.2 [M + H]⁺.

3-((3-(diphenylmethylene)-2-oxoindolin-1-yl)methyl)benzoic acid (3n): yellow crystalline solid in 91% yield; mp 230–232°C (decomp.); ¹H NMR (400 MHz, DMSO-*d*₆) δ (ppm): 7.90 (s, 1H), 7.84 (d, *J* = 7.6 Hz, 1H), 7.55 (t, *J* = 7.4 Hz, 1H), 7.53–7.50 (m, 3H), 7.47 (t, *J* = 7.7 Hz, 1H), 7.38–7.31 (m, 7H), 7.13 (t, *J* = 7.7 Hz, 1H), 6.91 (d, *J* = 7.8 Hz, 1H), 6.66 (t, *J* = 7.6 Hz, 1H), 6.16 (d, *J* = 7.7 Hz, 1H), 4.97 (s, 2H); ¹³C NMR (100 MHz, DMSO-*d*₆) δ (ppm): 167.55, 166.16, 154.63, 142.45, 141.56, 140.18, 137.79, 132.17, 131.69, 130.19, 129.69, 129.51, 129.43, 129.19, 128.91, 128.77, 128.49, 128.16, 123.94, 123.06, 122.99, 121.81, 109.30, 42.66; MS (ESI) m/z 432.2 [M + H]⁺.

(E)-3-((3-((4-chlorophenyl)(phenyl)methylene)-2-oxoindolin-1-yl)methyl)benzoic acid, C24 (3o): yellow crystalline solid in 88% yield; mp 204–206°C (decomp.); ¹H NMR (400 MHz, DMSO-*d*₆) δ (ppm): 7.91 (s, 1H), 7.85 (d, *J* = 7.7 Hz, 1H), 7.60–7.54 (m, 3H), 7.47 (t, *J* = 7.7 Hz, 1H), 7.40–7.30 (m, 7H), 7.15 (t, *J* = 7.8 Hz, 1H), 6.92 (d, *J* = 7.8 Hz, 1H), 6.73 (t, *J* = 7.5 Hz, 1H), 6.29 (d, *J* = 7.7 Hz, 1H), 4.97 (s, 2H); ¹³C NMR (100 MHz, DMSO-*d*₆) δ (ppm): 167.55, 166.04, 152.98, 142.55, 140.27, 139.91, 137.75, 134.48, 132.22, 131.59, 131.16, 130.32, 129.81, 129.44, 129.36, 128.79, 128.53, 128.24, 124.29, 122.96, 122.81, 122.00, 109.43, 42.66; MS (ESI) m/z 466.2 [M + H]⁺.

(Z)-3-((3-((4-chlorophenyl)(phenyl)methylene)-2-oxoindolin-1-yl)methyl)benzoic acid (3p): yellow crystalline solid in 89% yield; mp 211–213°C; ¹H NMR (400 MHz, DMSO-*d*₆) δ (ppm): 7.92 (s, 1H), 7.85 (d, *J* = 7.7 Hz, 1H), 7.57 (d, *J* = 7.8 Hz, 1H), 7.54–7.50 (m, 3H), 7.47 (t, *J* = 7.7 Hz, 1H), 7.42 (d, *J* = 8.6 Hz, 2H), 7.39–7.33 (m, 4H), 7.14 (t, *J* = 7.7 Hz, 1H), 6.92 (d, *J* = 7.8 Hz, 1H), 6.67 (t, *J* = 7.6 Hz, 1H), 6.20 (d, *J* = 7.6 Hz, 1H), 4.97 (s, 2H); ¹³C NMR (100 MHz, DMSO-*d*₆) δ (ppm): 167.55, 166.16, 152.83, 142.57, 141.07, 138.99, 137.74, 134.02, 132.22, 132.08, 131.64, 129.84, 129.77, 129.74, 129.44, 129.00, 128.81, 128.57, 128.27, 124.47, 123.07, 122.87, 121.91, 109.41, 42.71; MS (ESI) m/z 466.2 [M + H]⁺.

Biology

For the development of a cellular test system suitable for testing the ability of small molecule compounds to activate AMPK, the AMPKAR construct kindly provided by Lewis Cantley (Addgene plasmid #35097) was used.^[19] The construct was cloned into the pEYFP-N2 vector, which was transfected into H1299 cells (non-small cell lung cancer); expressing cells were selected with Geneticin (G-418, Gibco). The most stable clones with the maximum fluorescence at 477 nm were used as a basis for the cellular test system. Transfected cells were cultured in DMEM (Gibco) supplemented with 10% FBS, 2 mM L-glutamine, 100 U/mL penicillin, and 100 µg/mL streptomycin at 37°C in an atmosphere of 5% CO₂.

To evaluate the activity of the studied compounds, the cells were plated in FluoroBrite DMEM medium (Gibco) supplemented with 10% FBS and 2 mM L-glutamine on a 96-well plate with opaque black walls (Greiner). The studied compounds were dissolved in DMSO prior to the experiment. Detection of the fluorescent signal was performed on the Operetta High-Content Imaging System (Perkin Elmer); three channels were used for the detection of FRET signal (excitation filter 410–430 nm, emission filter 520–560 nm), CFP fluorescence (excitation filter 410–430 nm, emission filter 460–500 nm) and YFP fluorescence (excitation filter 490–510 nm, emission filter 520–560 nm). The first time point corresponded to the untreated cells; immediately after the measurement of the first time point the solution of the studied compounds was added to each well to the final concentration of 1 mM (6 wells per compound). The same amount of DMSO was used as a control (6 control wells). The plate was kept at 37°C in an atmosphere of 5% CO₂ during the experiment. The experiment was performed in triplicate.

The obtained images were processed using Harmony 3.1 software (Perkin Elmer). The cells were defined by intense fluorescence in the YFP fluorescence channel. The FRET effect was calculated by the ratio of mean FRET fluorescence intensity to mean CFP fluorescence intensity; eight most representative fields were processed in each well. All the obtained values were normalized. The activating effect of the studied compounds was assessed by the maximum change in the FRET effect (ΔFRET), observed after 50 min of the experiment.

Western blot analysis in H1299 cells untreated or treated with compounds (0.1 mM for 1 h) was performed on cell lysates centrifuged and resolved by SDS-PAGE. The separated proteins were transferred to a PVDF membrane and immunoblotted with specific antibodies according to the manufacturer's recommendations. The following antibodies were used in the work: phospho-AMPK alpha-1 (Thr172) polyclonal antibody (PA5-17831, Invitrogen), AMPK alpha-1 polyclonal antibody (PA5-29615, Invitrogen), phospho-Acetyl-CoA Carboxylase (Ser79) (D7D11) monoclonal antibody (#11818, Cell Signaling), anti-Acetyl Coenzyme A Carboxylase monoclonal antibody (ab45174, Abcam), phospho-Raptor (Ser792) polyclonal antibody (PA5-17116, Invitrogen), Raptor monoclonal antibody (H.558.9) (MA5-15051, Invitrogen), anti-GAPDH antibody (ab9484, Abcam). The primary antibodies were detected using Peroxidase conjugated anti-Rabbit IgG antibodies (A9169, Sigma-Aldrich) and anti-Mouse IgG (Fab specific)-Peroxidase antibodies (A9917, Sigma-Aldrich). The chemiluminescence intensity was evaluated using Novex ECL Chemiluminescent Substrate Reagent Kit (Invitrogen) in the ChemiDoc Imaging System (BioRad).

Acknowledgements

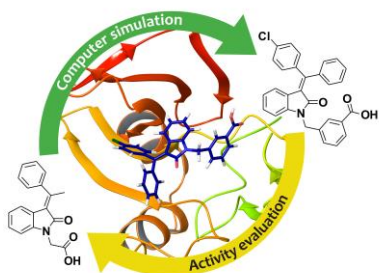
This work was financially supported by the Russian Science Foundation (project no. 16-13-10358). The authors also thank M. A. Gureev for calculations and A. V. Garabadzhiu for useful discussion.

Keywords: AMPK • FRET • high-content screening • molecular modeling • structure-activity relationships

References:

- [1] D. G. Hardie, M. L. Ashford, *Physiology (Bethesda)* **2014**, *29*, 99-107.
- [2] a) M. Gasparri, F. Giampieri, J. M. Alvarez Suarez, L. Mazzoni, T. Y. Forbes Hernandez, J. L. Quiles, P. Bullon, M. Battino, *Curr. Drug Targets* **2016**, *17*, 865-889; b) D. Carling, *Curr. Opin. Cell Biol.* **2017**, *45*, 31-37.
- [3] R. Ke, Q. Xu, C. Li, L. Luo, D. Huang, *Cell. Biol. Int.* **2018**, *42*, 384-392.
- [4] D. G. Hardie, D. Carling, V. A. Zammit, *FEBS Lett.* **1987**, *223*, 217-222.
- [5] I. Pernicova, M. Korbonits, *Nat. Rev. Endocrinol.* **2014**, *10*, 143-156.
- [6] a) B. Xiao, R. Heath, P. Saiu, F. C. Leiper, P. Leone, C. Jing, P. A. Walker, L. Haire, J. F. Eccleston, C. T. Davis, S. R. Martin, D. Carling, S. J. Gamblin, *Nature* **2007**, *449*, 496-500; b) B. Xiao, M. J. Sanders, E. Underwood, R. Heath, F. V. Mayer, D. Carmena, C. Jing, P. A. Walker, J. F. Eccleston, L. F. Haire, P. Saiu, S. A. Howell, R. Aasland, S. R. Martin, D. Carling, S. J. Gamblin, *Nature* **2011**, *472*, 230-233.
- [7] a) R. A. Srivastava, S. L. Pinkosky, S. Filippov, J. C. Hanselman, C. T. Cramer, R. S. Newton, *J. Lipid Res.* **2012**, *53*, 2490-2514; b) W. Li, S. M. Saud, M. R. Young, G. Chen, B. Hua, *Oncotarget* **2015**, *6*, 7365-7378.
- [8] M. F. Calabrese, F. Rajamohan, M. S. Harris, N. L. Caspers, R. Magyar, J. M. Withka, H. Wang, K. A. Borzilleri, P. V. Sahasrabudhe, L. R. Hoth, K. F. Geoghegan, S. Han, J. Brown, T. A. Subashi, A. R. Reyes, R. K. Frisbie, J. Ward, R. A. Miller, J. A. Landro, A. T. Londregan, P. A. Carpino, S. Cabral, A. C. Smith, E. L. Conn, K. O. Cameron, X. Qiu, R. G. Kurumbail, *Structure* **2014**, *22*, 1161-1172.
- [9] a) D. S. Novikova, A. V. Garabadzhiu, G. Melino, N. A. Barlev, V. G. Tribulovich, *Russ. Chem. Bull.* **2015**, *64*, 1497-1517; b) Novikova D.S., Ivanov G.S., Garabadzhiu A.V., Tribulovich V.G. in *Chemistry and Technology of Plant Substances: Chemical and Biochemical Aspects* (Eds.: A. V. Kutchin, L. N. Shishkina, L. I. Weisfeld), Apple Academic Press, New Jersey, **2017**, pp. 181-209.
- [10] J. E. Gómez-Galeno, Q. Dang, T. H. Nguyen, S. H. Boyer, M. P. Grote, Z. Sun, M. Chen, W. A. Craigo, P. D. van Poelje, D. A. MacKenna, E. E. Cable, P. A. Rolzin, P. D. Finn, B. Chi, D. L. Linemeyer, S. J. Hecker, M. D. Erion, *ACS Med. Chem. Lett.* **2010**, *1*, 478-482.
- [11] O. Mirquet, S. Sautet, C.-A. Clément, J. Toum, F. Donche, C. Marques, E. Rondet, M. Pizzonero, B. Beauvais, Y. Dudit, P. Huet, L. Trotter, P. Grondin, J.-M. Brusq, E. Boursier, Y. Saintillan, E. Nicodeme, *ACS Med. Chem. Lett.* **2013**, *4*, 632-636.
- [12] E. Meltzer-Mats, G. Babai-Shani, L. Pasternak, N. Uritsky, T. Getter, O. Viskind, J. Eckel, E. Cerasi, H. Senderowitz, S. Sasson, A. Gruzman, *J. Med. Chem.* **2013**, *56*, 5335-5350.
- [13] L. Chen, F. J. Xin, J. Wang, J. Hu, Y. Y. Zhang, S. Wan, L. S. Cao, C. Lu, P. Li, S. F. Yan, D. Neumann, U. Schlattner, B. Xia, Z. X. Wang, J. W. Wu, *Nature* **2013**, *498*, E8-10.
- [14] a) G. H. Zheng, J. J. Shen, Y. C. Zhan, H. Yi, S. T. Xue, Z. Wang, X. Y. Ji, Z. R. Li, *Eur. J. Med. Chem.* **2014**, *81*, 277-288; b) A. Pal, A. Ganguly, A. Ghosh, M. Yousuf, B. Rathore, R. Banerjee, S. Adhikari, *ChemMedChem* **2014**, *9*, 727-732.
- [15] a) T. A. Grigoreva, D. S. Novikova, M. A. Gureev, A. V. Garabadzhiu, V. G. Tribulovich, *Chirality* **2018**, *30*, 785-797; b) T. A. Grigoreva, D. S. Novikova, A. V. Petukhov, M. A. Gureev, A. V. Garabadzhiu, G. Melino, N. A. Barlev, V. G. Tribulovich, *Bioorg. Med. Chem. Lett.* **2017**, *27*, 5197-5202; c) T. A. Grigoreva, A. V. Garabadzhiu, V. G. Tribulovich, *Russ. J. Gen. Chem.* **2016**, *86*, 2454-2461; d) D. D. Orlova, D. S. Novikova, A. V. Garabadzhiu, V. G. Tribulovich, *Russ. J. Gen. Chem.* **2018**, *88*, 48-56.
- [16] P. Li, M. Zhao, A. B. Parris, X. Feng, X. Yang, *Biochem. Biophys. Res. Commun.* **2015**, *464*, 1267-1274.
- [17] a) T. Pang, B. Xiong, J. Y. Li, B. Y. Qiu, G. Z. Jin, J. K. Shen, J. Li, *J. Biol. Chem.* **2007**, *282*, 495-506; b) L. Chen, Z. H. Jiao, L. S. Zheng, Y. Y. Zhang, S. T. Xie, Z. X. Wang, J. W. Wu, *Nature* **2009**, *459*, 1146-1149.
- [18] N. Komatsu, K. Aoki, M. Yamada, H. Yukinaga, Y. Fujita, Y. Kamioka, M. Matsuda, *Mol. Biol. Cell.* **2011**, *22*, 4647-4656.
- [19] P. Tsou, B. Zheng, C. H. Hsu, A. T. Sasaki, L. C. Cantley, *Cell Metab.* **2011**, *13*, 476-486.
- [20] D. Durocher, I. A. Taylor, D. Sarbassova, L. F. Haire, S. L. Westcott, S. P. Jackson, S. J. Smerdon, M. B. Yaffe, *Mol. Cell.* **2000**, *6*, 1169-1182.
- [21] a) N. K. LeBrasseur, M. Kelly, T. S. Tsao, S. R. Farmer, A. K. Saha, N. B. Ruderman, E. Tomas, *Am. J. Physiol. Endocrinol. Metab.* **2006**, *291*, E175-181; b) G. Zadra, C. Photopoulos, S. Tyekucheva, P. Heidari, Q. P. Weng, G. Fedele, H. Liu, N. Scaglia, C. Priolo, E. Sicinska, U. Mahmood, S. Signoretti, N. Birnberg, M. Loda, *EMBO Mol. Med.* **2014**, *6*, 519-538.
- [22] N. Rozentul, Y. Avrahami, M. Shubely, L. Levy, A. Munder, G. Cohen, E. Cerasi, S. Sasson, A. Gruzman, *Pharm. Res.* **2017**, *34*, 2873-2890.
- [23] J. T. Siqueira, E. Batistela, M. P. Pereira, V. C. da Silva, P. T. de Sousa Junior, C. M. Andrade, N. H. Kawashita, G. L. Bertolini, A. M. Baviera, *Pharm. Biol.* **2016**, *54*, 1671-1679.
- [24] O. Fedorova, A. Daks, V. Petrova, A. Petukhov, L. Lezina, O. Shuvalov, P. Davidovich, D. Kriger, E. Lomert, D. Tentler, V. Kartsev, B. Uyanik, V. Tribulovich, O. Demidov, G. Melino, N.A. Barlev, *Cell Cycle* **2018**, *17*, 1917-1930.
- [25] a) M. Kravasin, M.A. Gureyev, D. Dar'ın, O. Bakulina, M. Chizhova, A. Lepikhina, D. Novikova, T. Grigoreva, G. Ivanov, A. Zhumagalieva, A.V. Garabadzhiu, V.G. Tribulovich, *Bioorg. Med. Chem.* **2018**, *26*, 2651-2673; b) T. Grigoreva, A. Romanova, A. Sagaidak, S. Vorona, D. Novikova, V. Tribulovich, *Bioorg. Med. Chem. Lett.* **2020**, *30*, 127424.
- [26] J. Carretero, P. P. Medina, R. Blanco, L. Smit, M. Tang, G. Roncador, L. Maestre, E. Conde, F. Lopez-Rios, H. C. Clevers, M. Sanchez-Céspedes, *Oncogene* **2007**, *26*, 1616-1625.
- [27] A. Chatterjee, G. Villarreal Jr., D.-J. Oh, M. H. Kang, D. J. Rhee, *Invest. Ophthalmol. Vis. Sci.* **2014**, *55*, 3127-3139.
- [28] H. Zimmermann, *Naunyn Schmiedebergs Arch. Pharmacol.* **2000**, *362*, 299-309.
- [29] a) F. A. Ross, T. E. Jensen, D. G. Hardie, *Biochem J.* **2016**, *473*, 189-199; b) M. Suter, U. Riek, R. Tuerk, U. Schlattner, T. Wallimann, D. Neumann, *J. Biol. Chem.* **2006**, *281*, 32207-32216.
- [30] T. Pang, Z. S. Zhang, M. Gu, B. Y. Qiu, L. F. Yu, P. R. Cao, W. Shao, M. B. Su, J. Y. Li, F. J. Nan, J. Li, *J. Biol. Chem.* **2008**, *283*, 16051-16060.
- [31] L. F. Yu, Y. Y. Li, M. B. Su, M. Zhang, W. Zhang, L. N. Zhang, T. Pang, R. T. Zhang, B. Liu, J. Y. Li, J. Li, F. J. Nan, *ACS Med. Chem. Lett.* **2013**, *4*, 475-480.
- [32] Y. Y. Li, L. F. Yu, L. N. Zhang, B. Y. Qiu, M. B. Su, F. Wu, D. K. Chen, T. Pang, M. Gu, W. Zhang, W. P. Ma, H. W. Jiang, J. Y. Li, F. J. Nan, J. Li, *Toxicol. Appl. Pharmacol.* **2013**, *273*, 325-334.
- [33] X. Li, L. Wang, X. E. Zhou, J. Ke, P. W. de Waal, X. Gu, M. H. Tan, D. Wang, D. Wu, H. E. Xu, K. Melcher, *Cell Res.* **2015**, *25*, 50-66.
- [34] M. Gureev, D. Novikova, T. Grigoreva, S. Vorona, A. Garabadzhiu, V. Tribulovich, *J. Comput. Aided Mol. Des.* **2020**, *34*, 55-70.
- [35] L. De Colibus, X. Wang, J. A. B. Spyrou, J. Kelly, J. Ren, J. Grimes, G. Puerstinger, N. Stonehouse, T. S. Walter, Z. Hu, J. Wang, X. Li, W. Peng, D. J. Rowlands, E. E. Fry, Z. Rao, D. I. Stuart, *Nat. Struct. Mol. Biol.* **2014**, *21*, 282-288.
- [36] F. Nan, L. Yu, M. Zhang, L. Chen, M. Huang, L. Feng, J. Li, T. Pang, (Hoffmann-La Roche Inc., Nutley, USA), US Patent No. US 8,778,973 B2, **2014**.
- [37] D. S. Novikova, T. A. Grigoreva, A. A. Zolotarev, A. V. Garabadzhiu, V. G. Tribulovich, *RSC Advances* **2018**, *8*, 34543-34551.
- [38] G. Jones, P. Willett, R. C. Glen, A. R. Leach, R. Taylor, *J. Mol. Biol.* **1997**, *267*, 727-748.
- [39] I. V. Tetko, P. Bruneau, *J. Pharm. Sci.* **2004**, *93*, 3103-3110.
- [40] C. Crestini, R. Saladino, *Synth. Commun.* **1994**, *24*, 2835-2841.

Entry for the Table of Contents



The binding site of 3-benzylidene oxindoles within the AMPK kinase domain was established by correlating calculated and experimental activities. Such binding to the kinase domain leads to the AMPK activation. The cell model based on the FRET effect was used under HCS conditions to evaluate the target activity.